Three-Dimensional Structure of a Nanocomposite Material Consisting of Two Kinds of Nanofillers and Rubbery Matrix Studied by Transmission Electron Microtomography

ARTICLE *in* MACROMOLECULES · AUGUST 2007

Impact Factor: 5.8 · DOI: 10.1021/ma071102d

6 AUTHORS, INCLUDING:

Hiroshi Jinnai
Tohoku University
234 PUBLICATIONS **4,233** CITATIONS
SEE PROFILE

Keizo Akutagawa
Bridgestone Corporation
14 PUBLICATIONS **71** CITATIONS
SEE PROFILE

Toshio Nishi
Tokyo Institute of Technology
216 PUBLICATIONS **4,762** CITATIONS
SEE PROFILE

Three-Dimensional Structure of a Nanocomposite Material Consisting of Two Kinds of Nanofillers and Rubbery Matrix Studied by Transmission Electron Microtomography

Hiroshi Jinnai,*,† Yuki Shinbori,† Tatsuro Kitaoka,† Keizo Akutagawa,‡ Naruhiko Mashita,‡ and Toshio Nishi§

Department of Macromolecular Science and Engineering, Graduate School of Science and Engineering, Kyoto Institute of Technology, Matsugasaki, Kyoto 606-8585, Japan; Bridgestone Corporation, 3-1-1, Ogawahigashi-Cho, Kodaira-Shi, Tokyo 187-8531, Japan; and Department of Organic and Polymeric Materials, School of Science and Engineering, Tokyo Institute of Technology, 2-12-1, Ohokayama, Meguro-ku, Tokyo 152-8552, Japan

Received May 16, 2007; Revised Manuscript Received June 18, 2007

ABSTRACT: The three-dimensional (3D) morphology of particulate fillers embedded in a rubbery matrix was examined by transmission electron microtomography (TEMT). Two types of nanofillers, i.e., carbon black (CB) and silica (Si) nanoparticles, were used as the nanofillers. Although the CB and Si nanoparticles were difficult to distinguish by conventional transmission electron microscopy (TEM), they appeared different by TEMT; the CB and Si nanoparticles appeared to be hollow and solid particles in the cross-sectional images of the TEMT 3D reconstruction, respectively, demonstrating that TEMT itself provided a unique particle-discriminative function. The nanoparticles were found to form aggregates in the matrix. It is intriguing that each aggregate was made of only one species; not a single aggregate contained both the CB and Si nanoparticles. A particle-packing algorithm was developed to estimate the positions of each primary nanoparticle inside the aggregates.

I. Introduction

Organic−inorganic nanometer composites have attracted substantial interest from researchers since they often exhibit unexpected properties synergistically derived from the two components. Composite systems based on organic polymers and inorganic clay minerals have been extensively studied due to their mechanical,[1,2] gas barrier properties, etc. Nanometer size particulate fillers, e.g., carbon black (CB), silica (Si) nanoparticles, etc., also form hybrids with organic polymers. They show a significant increase in both their static and dynamic moduli,[3] strength,[4] and thermal and electrical conductivity.[5,6] For example, there exists a certain volume fraction of CB, called the percolation threshold,[7] above and below which the composite behaves essentially like an electric conductor and an insulator, respectively. Such a sharp macroscopic transition is believed to have something to do with the internal organization of the CB within the polymer matrix. Above the percolation threshold, a continuous interconnecting CB network may exist throughout the material. Likewise, the interconnecting CB network is also believed to be the cause of the large mechanical strength of the CB-filled polymer. Thus, it is important to understand the structure−property relationship in order to achieve better mechanical or electrical properties in the CB/polymer composite.

Currently, more than one species of nanofillers are introduced into a polymer matrix. One typical example is a composite of CB and Si nanoparticles in a rubbery matrix. In this composite, the CB increases the strength of the elastomer[8,9] and thus acts as reinforcing fillers as described above, while the Si nanoparticles may add tear strength, abrasion resistance, and a reduction in the heat built up. In order to improve and maximize such functionalities, it is first necessary to *independently* visualize the two different kinds of fillers in the matrix and to determine their three-dimensional (3D) spatial distributions.

Until now, the filled polymers have been observed by transmission electron microscopy (TEM) and other experimental techniques, e.g., scattering methods.[10] There are, however, several experimental difficulties for an accurate structural analysis: (i) As shown later (in Figure 1), it is often difficult to distinguish the CB from the Si nanoparticles by TEM in spite of their relatively large electron-density difference. Even though the fillers are discernible in principle by TEM, since there is an overlap of the fillers in the depth direction (direction parallel to the optic axis of the microscope), in reality, it is quite difficult to distinguish one filler from the other. (ii) TEM provides only a two-dimensional (2D) projection of a 3D structural body. For the former problem, electron energy loss spectroscopy (EELS),[11] which enables us to obtain an elemental-mapped image, would be useful. For the latter problem, transmission electron microtomography (TEMT),[12−16] which provides 3D images in a nanometer resolution, should be a solution. Recently, TEMT has been used to investigate block copolymer morphologies,[17−25] a nanofibrillar network in a polymer matrix,[26] metal/zeolite crystals,[27] and filler/rubber systems.[28,29] Note that the EELS can be used together with the TEMT (TEMT-EELS) that will provide elemental-mapped 3D image of materials. In the present study, nanocomposites consisting of both CB and Si nanoparticles in rubbery matrices were examined by TEMT and TEMT-EELS in order to *independently* visualize the CB and Si nanoparticles and then study the spatial distributions of the fillers.

II. Experimental Section

A. Materials. The CB and Si nanoparticles used in the present study were purchased from Tokai Carbon Co., Ltd., and Nippon Silica Industrial Co., Ltd., respectively. The two kinds of particles

* To whom correspondence should be addressed: e-mail: hjinnai@kit.ac.jp.
† Kyoto Institute of Technology.
‡ Bridgestone Corporation.
§ Tokyo Institute of Technology.

10.1021/ma071102d CCC: $37.00
Published on Web 08/11/2007

were dispersed on TEM Cu grids and were observed by TEM. The average diameters of the CB and Si nanoparticles were determined from the TEM experiments to be 23.3 and 20 nm, respectively. It was also found from the TEM observations that the CB had a relatively broad bimodal size distribution that peaked at ca. 20 and 25 nm. A mixture of natural rubber (NR) and polybutadiene (BR) was used as a rubbery matrix. A weight-average molecular weight, M_w, and a molecular weight distribution, M_w/M_n, of the NR were 1800K g/mol and 3.5−5.0, respectively. The M_w and M_w/M_n of the BR were 500K g/mol and 2.2, respectively. The BR was obtained from UBE Industries, Ltd. The NR is Ribbed smoked sheets grade 3.

B. Specimens. Two kinds of fillers, i.e., the CB and Si nanoparticles, were dispersed in the mixture of NR and BR (NR/BR = 60/40 wt %) in the following way. During the first stage of mixing, master batches with polymers, fillers, and a small amount of silane coupling agents, bis(3-triethoxylsililpropyl)tetrasulfide, were mixed in a mixer at 160 °C. Subsequently, the curing agents such as stearic acid, zinc oxide, a vulcanization accelerator, and sulfur in small quantities were added to the master batches in the mixer. These stocks were cured at 145 °C for 40 min. The volume fractions of the CB and Si nanoparticles were 6.5 and 6.2%, respectively. We hereafter call the specimen the CB&SI/NRBR.

C. Sample Preparation for Transmission Electron Microtomography. Ultrathin sections were prepared using a focused ion beam (FIB) at cryogenic temperature (∼−120 °C).[30] The obtained ultrathin sections, having a thickness of ca. 130 nm, were transferred to the TEM copper grid coated with a substrate. Prior to the TEMT observations, a small amount of gold colloidal solution (GCN005, BBInternational Ltd., UK) was dropped on the ultrathin sections. After evaporating the solvent (water), gold particles (5 nm in diameter) were left on the surface of the sections. They were used as fiducial markers for the alignment of the tilt series of the TEM images.[13]

D. Transmission Electron Microtomography (TEMT). In the TEMT experiments, a tilt series of 121 images were taken from +60° to −60° in 1° increments at a magnification of 25K using a JEOL JEM-2200FS microscope operated at 200 kV with 2048 × 2048 pixel elements (Gatan USC1000, Gatan Inc.). The pixel size of the projection was 0.412 nm. The exposure time for each projection was 6 s. In order to obtain achromatic projections, only the transmitted and elastically scattered electrons (electron energy loss: 0 ± 30 eV) were selected by an energy filter installed in the JEM-2200FS (Ω filter, JEOL Ltd., Tokyo, Japan) ("zero-loss" imaging).

As a crucial prelude to compute the 3D reconstruction, an alignment of the tilt series was first necessary because of the uncontrolled and magnification-dependent rotation of the projection by the electron optics within the microscope.[13] An area common to each projection in the tilt series was utilized to perform the alignment by tracing the motions of several fiducial points, i.e., the gold particles, in the area.[13] Note that the mean alignment error,[18] averaged over all of the fiducial markers used in the alignment, was 0.126 nm, which was less than the pixel resolution regardless of the tilt angles.[31] The tilt series after the alignment was subsequently reconstructed by the filtered back-projection algorithm.[32] For the alignment and 3D reconstruction, we developed homemade programs based on earlier algorithms published.[33,34]

E. TEMT−EELS. In order to observe the 3D distribution of only the Si nanoparticles, electron energy loss spectroscopy (EELS) was used together with TEMT. In EELS, some of the incoming electrons to the specimen lose electron energy that is specific to each element. Thus, selecting electrons with a particular electron energy loss, ΔE, corresponding to a specific element before the imaging system of the microscope produces a 2D projection of the element. In the case of Si, ΔE is 99 eV (Si L-edge) and 1839 eV (Si K-edge). Since the image intensity of the energy loss electrons of the K-edge was substantially lower than that of the L-edge, we used the L-edge to minimize the exposure time.

In the EELS imaging, two projections at a smaller electron energy loss than ΔE ("preedge" projections) are required to estimate the background energy spectrum, which will be subtracted from the projection at ΔE ("postedge" image) in the same area ("three-window method"). One of the biggest experimental difficulties is the beam damage to the sample. Hence, in the present study, in order to minimize the electron dose on the sample, the Si-mapped projections were generated by simply taking a ratio of the "postedge" ($\Delta E = 119 \pm 20$ eV) to "preedge" ($\Delta E = 87 \pm 20$ eV) projections in the same area of the sections ("two-window method"). Note that the two-window method provides only the position of an element (in our case, Si), while the three-window method theoretically gives the concentration of Si.

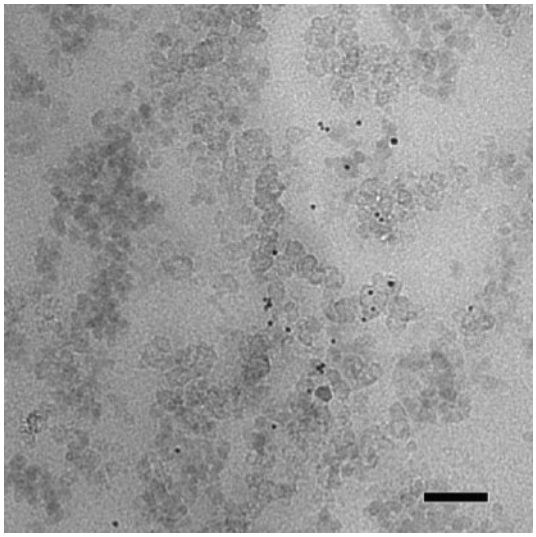

Figure 1. A TEM micrograph (zero-loss image) of CB&Si/NRBR. Particles with diameters around 20 nm are either the CB or Si nanoparticles, which is difficult to distinguish in this TEM micrograph alone. The dark small dots are gold particles used for alignment of the tilt series. Bar shows 100 nm.

A series of Si-mapped projections were taken in the way similar to the TEMT experiments, except for a couple of experimental conditions: First, the angular increment was set to 10° instead of 1°. The exposure times for the EELS images (both preedge and postedge images) were 10 s and were recorded with 512 × 512 pixel elements (1.67 nm/pixel) in order to attain as reasonable counting statistics as possible.

III. Results and Discussion

A. TEM Observation in the CB&Si/NRBR System. Figure 1 shows a TEM micrograph of ultrathin sections in the CB&Si/NRBR. The thickness of the section was ca. 130 nm (see section III.B and Figure 3). Some of the fillers may seem to be a little darker than the others. Since the electron densities of the CB and Si nanoparticles are 5.42×10^{23} and 5.87×10^{23} cm^{-3}, respectively, the Si nanoparticles should appear darker than the CB. The darker fillers in Figure 1 could be ascribed to the electron density difference, or they appeared darker simply due to the overlap along the depth direction. In any case, the difference between the two fillers under the TEM was not significant.

B. 3D Reconstruction in the CB&Si/NRBR System. Figure 2 shows volume-rendered 3D images viewed from different angles. It was observed that most of the fillers aggregated, which are further connected to each other to form the network structure.

The volume-rendered image is normally convenient to understand the global morphological features but is not appropriate for examining the subtle details of the morphology. One way to examine the 3D reconstruction in more detail is to examine a slice through the 3D reconstruction ("a digital slice"). Figure 3 shows an orthogonal cross-sectional view of the

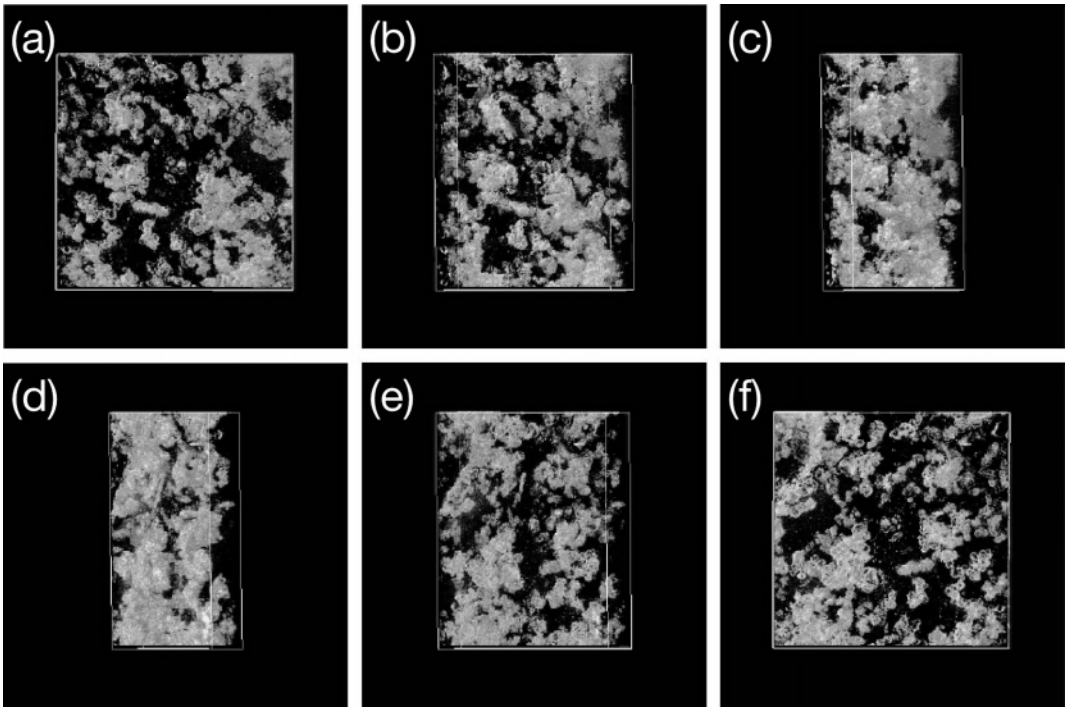

Figure 2. 3D reconstruction of CB&Si/NRBR from various viewing angles. White regions correspond to fillers. 3D reconstruction was made from zero-loss images at various angles ranging from +60° to −60°, and thus both the CB and Si nanoparticles are shown in the 3D images. The box size is 726 nm × 726 nm × 107 nm.

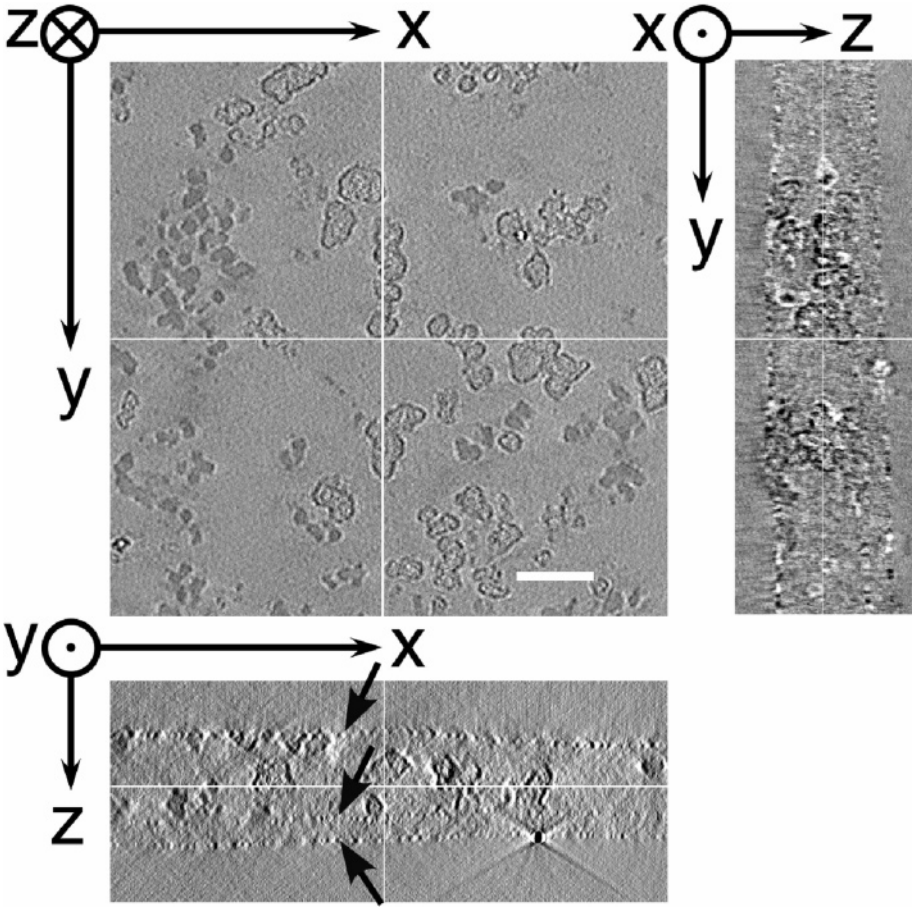

Figure 3. Orthogonal cross-sectional view of the CB&Si/NRBR system. The *Z*-axis is the direction parallel to the optical axis of the microscope and also to the sample thickness. The solid lines in each cross section indicate the position of the other two orthogonal sections. In the $X-Z$ cross section, the upper and lower edges of the section and the lower edge of the substrate are indicated by arrows, respectively, from top to bottom. The black dot in the lower right in the $X-Z$ cross section is the Au particle used for alignment. Scale bar shows 100 nm.

CB&Si/NRBR system, in which three digital slices from different directions are displayed. The $X-Z$ cross section is the plane where the filtered back projection was carried out. We emphasize here that the upper and lower edges of the sample

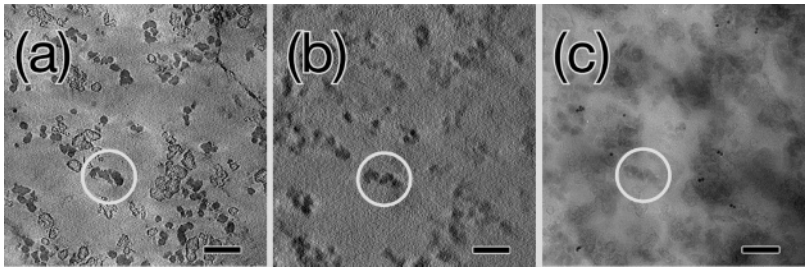

Figure 4. (a) A digital slice of TEMT, (b) A digital slice image of 3D reconstruction from TEMT-EELS, and (c) TEM micrograph in the same field of view of the CB&Si/NRBR system. White circles indicate the same aggregate, i.e., Si aggregate, in the three pictures. Bar shows 100 nm.

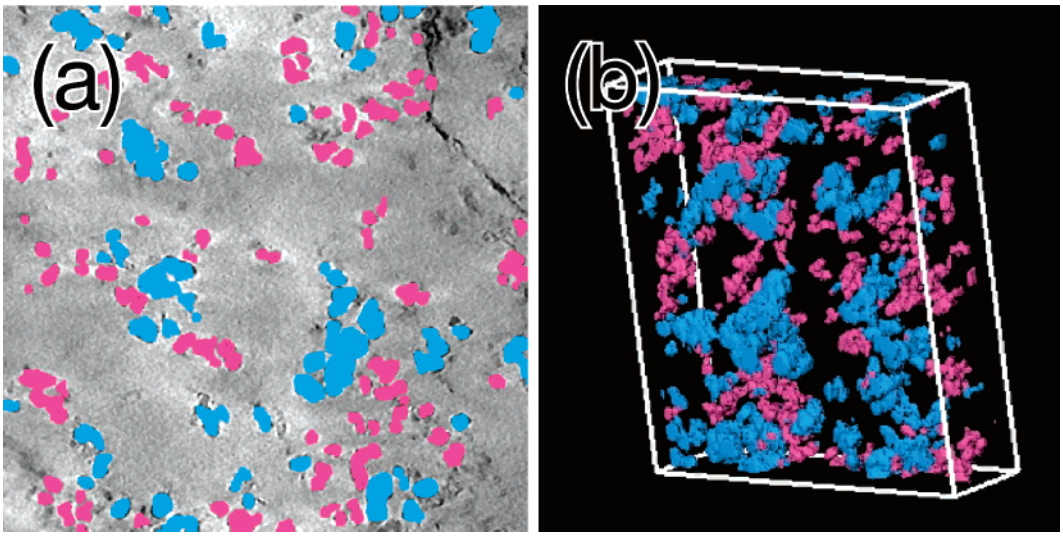

Figure 5. (a) Binarization of CB (blue) and Si nanoparticles (red). The digital slice is the same image as Figure 4a. (b) 3D reconstruction of the CB&Si/NRBR system. Box size is 726 nm × 726 nm × 107 nm. In both parts, the blue and red particles represent the CB and Si nanoparticles.

were clearly seen in the $X-Z$ plane, from which the thickness of the FIB-prepared section was evaluated to be ca. 130 nm. The lateral digital slice (a plane perpendicular to the optical axis of microscope, $X-Y$ cross section in Figure 3) of the CB&Si/NRBR system is again shown in Figure 4a. For comparison, the digital slices obtained from the TEMT-EELS experiment and TEM projection in the same field of view as in Figure 4a are displayed in parts b and c of Figure 4, respectively.

From the TEM micrograph (Figure 4c), it is possible to judge the extent of the dispersion of the fillers in the rubbery matrix. However, since the fillers overlapped along the depth direction and resolution along this direction is lost in the TEM, the identification of each filler was difficult. In contrast, the digital slice of the 3D reconstruction (Figure 4a) had a higher contrast than the TEM, and the detailed features, i.e., the spatial arrangements of the fillers, were well reproduced. Note that, although the original thickness of the section was ca. 130 nm, the thickness of the digital slice was effectively 1.7 nm, which eliminated overlap of the fillers along the depth direction. What is intriguing is that there are observed two kinds of fillers in Figure 4a: one appeared solid, while the other was rather transparent in the middle with their edges having a strong contrast, somewhat like hollow spheres. Assignment of these two kinds of particles to either the CB or to the silica particle is required in order to understand the morphology of the CB&Si/NRBR system, which will be discussed in the following section.

C. Identification of CB and Si Nanoparticles in 3D Reconstructed Images. The CB&Si/NRBR was examined by TEMT−EELS in order to identify the Si nanoparticles in the system. Note that the 3D reconstruction was carried out from the series of energy-filtered Si mapped projections in the TEMT−EELS experiment. Figure 4b shows digital slices of the 3D reconstruction, in which the black particles correspond to the Si nanoparticles.

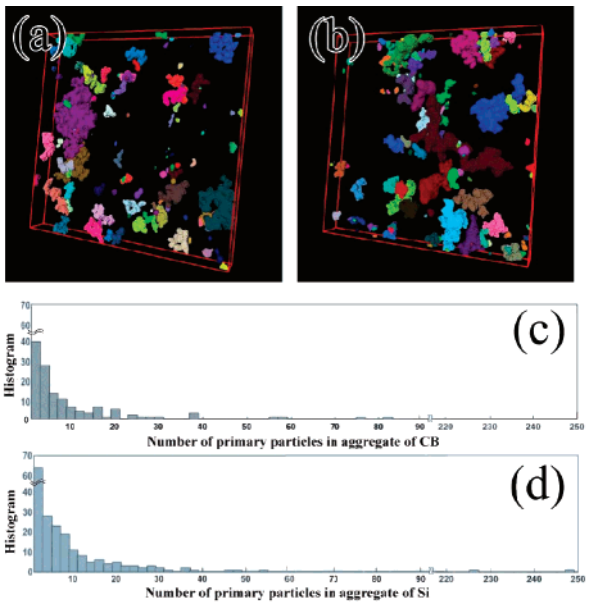

Figure 6. 3D images of (a) CB and (b) Si nanoparticles after the particle analysis. Different colors in each 3D image represent different aggregates. The box size is 726 nm × 726 nm × 107 nm for both 3D image. Parts c and d are histograms of aggregate volume for the CB and Si nanoparticles, respectively. Note that the volume of the aggregates is scaled by the volume of the primary particles. The diameters of CB and Si nanoparticles used for the scaling were 23.3 and 20 nm, respectively.

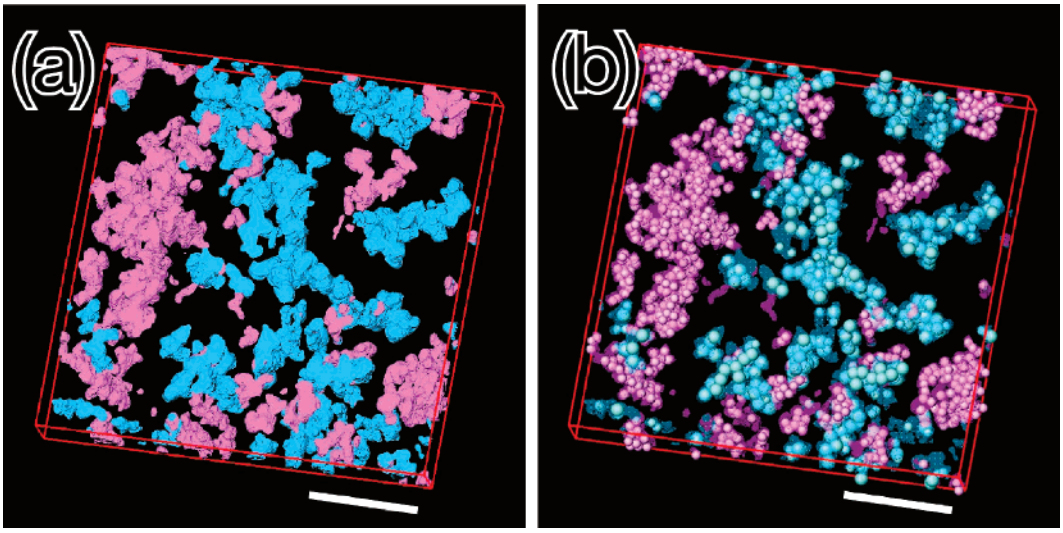

Figure 7. (a) 3D reconstruction of the CB&Si/NRBR system. Blue and red regions consist of CB and Si nanoparticles, respectively. The image is essentially the same as the one shown in Figure 5a. (b) 3D reconstruction of the CB&Si/NRBR system after the particle-packing analysis. The blue and red balls represent the CB and Si nanoparticles whose diameters are 25 and 20 nm, respectively. The CB and Si regions are translucent in part b. Bar shows 200 nm.

The image quality of the digital slice in the TEMT picture (Figure 4a) is better than that in the TEMT−EELS (Figure 4b) mainly due to the lower signal-to-noise ratio (S/N) of the Si-mapped projections and also due to the larger angular increment in the data acquisition of the TEMT−EELS experiment. Nevertheless, the position of the Si nanoparticles was clearly seen.

Comparing parts a and b of Figure 4, it was found that the aggregates of fillers marked by a circle in each part of Figure 4 were silica aggregates. In fact, a one-to-one correspondence was observed between the solid particles (or aggregates) in the TEMT digital slice and the Si nanoparticles (aggregates) in the TEMT−EELS data. Moreover, no fillers were observed in Figure 4b at the same position where the hollow particles existed in Figure 4a. Close examination of the two digital slices in such a way provides the following important result: Among the two kinds of fillers observed in Figure 4a, the hollow and solid particles are respectively the CB and Si nanoparticles. This experimental finding is particularly important because it demonstrates that the two kinds of fillers can be directly distinguished by TEMT. It is interesting to point out here that, even though we now know which fillers (or aggregates) are the CB or the Si nanoparticles, it is still difficult to distinguish these two kinds in the conventional TEM projection (see Figure 4c). The nature of the appearance of the CB in the digital slice of the TEMT experiment is not known at the time of this writing. However, the hollow particles of CB have been observed under TEM in the past, in which Heidenteich et al. proposed a model of a single CB particle with a concentric surface parallel orientation of ordered layer groupings and diminishing graphitic order near the particle center.[35] We suspect this might be the cause in the case of our TEMT observations.

D. Element-Specific Three-Dimensional Visualization of the CB&Si/NRBR System. Since the CB and Si nanoparticles were distinguished by TEMT (see section III.C), the arrangement of these two kinds of fillers can be directly visualized in the digital slices. Figure 5a is reproduced from the same digital slice presented in Figure 4a, in which the CB and Si nanoparticles are indicated by the blue and red colors, respectively. After such binarization in each digital slice, they are reconstructed into a 3D image,[36] as shown in Figure 5b. The volume fractions estimated from the 3D image for the CB and Si nanoparticles were 6.5% and 6.2%, respectively. These experimentally obtained numbers are in excellent agreement with the known compositions for the CB and Si nanoparticles, i.e., 7.7% and 6.2%, respectively. It was found that the aggregates consisted of only one species of the nanoparticles. Namely, the CB and Si aggregates are made only of the CB and Si nanoparticles, respectively.

The size of each aggregate can be measured by separating the aggregates one from the other using the particle analysis algorithm.[37] Parts a and b of Figure 6 demonstrate the results of such an analysis in which the individual aggregates are shown in different colors for the CB and Si nanoparticles, respectively. Once each aggregate is separated, various structural parameters characterizing the system, e.g., the volume, the center of mass, the shape, etc., of the aggregate can be measured.[37] The histograms of the volume of the aggregates are shown in parts c and d of Figure 6 for the CB and Si nanoparticles, respectively. The size distributions were similar between the two kinds of particles. Most of the aggregates were less than 10 particles, while some consisted of 70 or more. For a more accurate structural analysis, statistical averaging over a larger volume, i.e., averaging over many 3D volume data such as the one shown in Figure 5b, may be necessary. Such an analysis is now in progress. In addition, it would be important and deserves future studies to investigate the effect of matrix rubbers or surface modifications of nanoparticles on the size distribution of the aggregates.

E. Visualization of Primary Particles in the CB&Si/NRBR System. Although the 3D image shown in Figure 5b exhibits by far richer structural information itself than the TEM micrograph (see Figure 1), it only shows the outer shape of each aggregate. If one can estimate the spatial position of each primary particle, i.e., individual CB and Si nanoparticles, such structural information should be quite useful to correlate the internal morphology with various properties, e.g., the mechanical and electrical properties. For example, knowledge of the spatial arrangement of the nanoparticles in the composite can be employed to estimate the mechanical properties on the basis of a finite element analysis (FEA),[38−40] which would be a more accurate model than the conventional one where the nanoparticles have been *virtually* and *manually* arranged on the basis

of insufficient 2D TEM images. Moreover, the persistent length of each aggregate, an important measure to understand the electric conductivity of the nanocomposite materials, will be evaluated by examining the connectivity of the primary nanoparticles.[41]

In the present study, a "particle-packing" algorithm based on the Monte Carlo method (see Appendix for details) was used to virtually pack as many spherical particles as possible inside the aggregates. Figure 7 shows the 3D images of the CB&Si/NRBR system before and after the particle-packing analysis. The diameters of the CB and Si nanoparticles used in this simulation were 25 and 20 nm, respectively. These values were chosen from the peak of the size distributions of the particles obtained from the TEM experiments (not shown here). Note that smaller CB particles with a diameter of 20 nm were also filled after running the particle-packing algorithm with 25 nm spheres because there were several regions in which no CB particles were inserted if we only used 25 nm CB particles. The fraction of the small particles was ~30%, which roughly agreed with the size distribution of the CB.

The volume fractions of the CB and Si nanoparticles after the particle-packing analysis turned out to be 5.9% and 4.5%, which were smaller than the volume fractions evaluated from the 3D reconstructions shown in Figure 5a (see section III.D). This result indicates that the virtual CB and Si nanoparticles did not fully occupy the corresponding regions, demonstrating that the particle-packing algorithm is semiquantitaive. Considering the fact that the CB and Si nanoparticles are neither perfect spheres nor monodispersed, we regarded that the agreement of the volume fraction before and after the particle-packing analysis was reasonably good. Most importantly, the shape of the aggregates was well preserved even after the particle-packing analysis, and thus the analysis provides an intuitive understanding of the distribution of the primary nanoparticles.

IV. Summary

The three-dimensional (3D) structure of a nanocomposite material consisting of two kinds of fillers in rubbery matrix was investigated by transmission electron microtomography (TEMT). The carbon black (CB) and silica (Si) nanoparticles were used as fillers. Using electron energy loss spectroscopy together with TEMT, it became possible to differentiate the two kinds of nanoparticles in the 3D reconstruction. The CB and Si nanoparticles appeared to be hollow and solid (filled) particles, respectively, in the digital slice that is a cross section of the 3D TEMT reconstructed data. It was found that both the CB and Si nanoparticles formed aggregates that consist of only one species. In other words, no aggregates were only a mixture of the CB and Si nanoparticles. The volume fractions of the two fillers obtained from the 3D reconstruction gave excellent agreement with the known compositions evaluated from the sample preparation. On the basis of such quantitative 3D volume data, a newly developed algorithm was used to evaluate the spatial distribution of the primary particles inside the aggregates. The virtual primary particles were nicely filled in the aggregates without changing their shapes. Considering that the fillers were treated as spheres with a single (or double) size distribution (in reality, they are neither spheres nor monodispersed in diameter), the volume fractions of the CB and Si nanoparticles were in reasonable agreement with the known volume fractions, indicating that the analysis is semiquantitative. The 3D visualization and structural analysis reported in the present study can be further used to evaluate the persistent length of the aggregates that should have a strong influence on the mechanical and electrical properties of the nanocomposite materials. The 3D data can also be used as a model for the FEA to directly simulate the mechanical properties. These analyses are currently in progress.

Acknowledgment. The authors are grateful to NEDO for support through the Japanese National Project "Nano-Structured Polymer Project" by the Ministry of Economy, Trade and Industry and for support from the Ministry of Education, Science, Sports and Culture through Grants-in-Aid No. 1855019 and No. 19031016. The authors thank Mr. H. Nishioka, JEOL Co., Ltd., for his useful discussions and help with the TEMT−EELS and TEMT experiments.

Appendix

Figure 8 is a close-up view of the TEMT image of a CB aggregate. It appeared that several CB primary particles were connected to make the aggregate. Thus, it is worth trying to represent the aggregates by the primary CB (or Si) particles in a sensible way. Such a "virtual model" based on the TEMT 3D reconstruction, even if it is semiquantitative, will offer a valuable path to estimate the variety of significant structural parameters related to the material properties of the nanocomposite, e.g., the spatial distribution and consistent length of the fillers. Moreover, the virtual model may be used as a reasonable model for the FEA to simulate the mechanical properties of the nanocomposite. We hereafter call the method a "particle-packing" method.

In the particle-packing method, the primary particles will be packed inside the regions consisting of either the CB or Si nanoparticles as closely as possible. In the present study, we used a geometrical approach based on the Monte Carlo method.[42] The primary particles are assumed to be spheres with a monodispersed distribution. Although, in reality both the CB and Si nanoparticles exhibit neither perfect spheres nor a monodisperse distribution, we used this condition for simplicity.

Let us now briefly explain the algorithm of our particle-packing method using the schematic drawing shown in Figure 9a. In Figure 9, the dark gray circles and light gray region represent respectively the virtual primary particles and experimentally obtained CB (or Si) region. In our method, the primary particles are not solid spheres but rather soft ones. We allowed a slight deformation for the particles (15 vol %). In other words, overlap of the particles is allowed if the overlapped volume is less than 15 vol % of the total volume of each particle.

The particle-packing method obeys the following protocol. First, a point in the TEMT 3D reconstructed image is randomly chosen, e.g., the black dot in Figure 9a. If the point is outside the filler regions (white regions in Figure 9a), the step is stopped (nothing happens). If the chosen point is inside the filler regions, but not occupied by another particle such as in the case shown in Figure 9a, a new primary particle is placed with the point as a center of the new primary particle (see Figure 9b). The volume of the primary particle outside the filler region, V_a, and that overlapped with other particles, V_b, are then evaluated. If the sum of these two volumes, $V_a + V_b$, exceeds 20 vol % of the volume of the primary particle, the particle is removed and a new point will be chosen. If the $V_a + V_b$ for the newly placed particle is less than 20 vol %, it is placed at that position and V_a and V_b for the existing particles are recalculated (since the incorporation of the new particle affects these volumes of the existing particles). The newly placed particle is then randomly

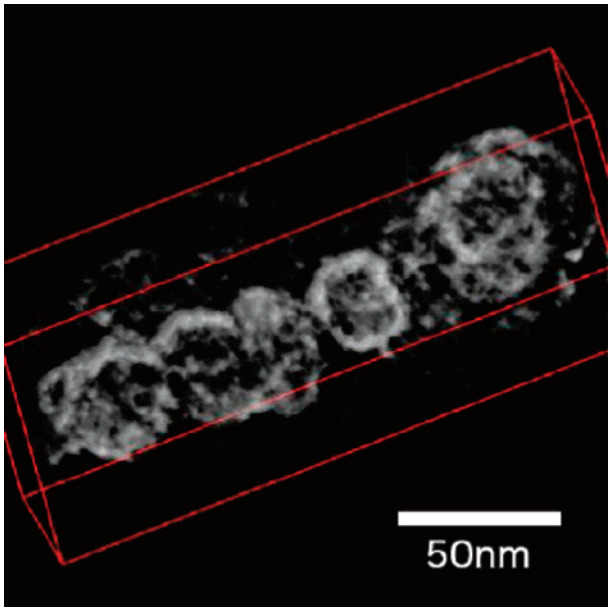

Figure 8. Close-up view of the TEMT image of a CB aggregate shown in a volume-rendered fashion.

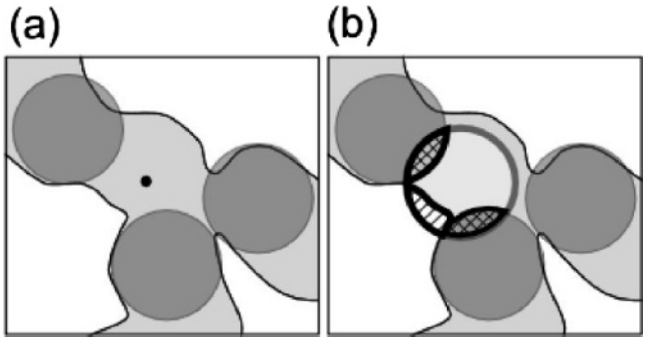

Figure 9. Schematic illustrations of the Monte Carlo step. For the simplicity, two-dimensional illustrations are displayed. The light and dark gray regions are respectively the CB region and CB primary particles. (a) A point is randomly chosen which is shown as the black dot. (b) A sphere is placed with the point being the center of the sphere. The overlaps with the other spheres, V_a, are shown as the cross-hatched region, and the volume outside the CB region, V_b, is shown as the shaded region.

moved (within the distance of $^1/_8$ of the diameter of the primary particle) in order for the $V_a + V_b$ at the new position to decrease to 15 vol %. Accordingly, the existing particles are also moved slightly so that they all have a $V_a + V_b$ value less than 15 vol %. Finally, the algorithm starts to look for a new position for the next primary particle. The Monte Carlo step is iteratively applied to the TEMT 3D reconstructed image until an additional sphere cannot be inserted during sufficiently many Monte Carlo steps (of the order of few million steps).

Supporting Information Available: Two QuickTime videos showing the 3D morphologies: (S1) element-specific 3D reconstruction of the CB&Si/NRBR system presented in Figure 5; (S2) 3D reconstruction of the CB&Si/NRBR system after the particle-packing analysis presented in Figure 7. This material is available free of charge via the Internet at http://pubs.acs.org.

References and Notes

(1) Kawasumi, M.; Hasegawa, N.; Kato, M.; Usuki, A.; Okada, A. *Macromolecules* **1997**, *30*, 6333−6338.
(2) Maiti, P.; Nam, P. H.; Okamoto, M.; Hasegawa, N.; Usuki, A. *Macromolecules* **2002**, *35*, 2042−2049.
(3) Busfield, J. J. C.; Deeprasertkul, C.; Thomas, A. G. *Polymer* **2000**, *41*, 9219−9225.
(4) Tsunoda, K.; Busfield, J. J. C.; Davies, C. K. L.; Thomas, A. G. *J. Mater. Sci.* **2000**, *35*, 5187−5198.
(5) Yamaguchi, K.; Busfield, J. J. C.; Thomas, A. G. *J. Polym. Sci., Part B: Polym. Phys.* **2003**, *41*, 2079−2167.
(6) Busfield, J. J. C.; Thomas, A. G.; Yamaguchi, K. *J. Polym. Sci., Part B: Polym. Phys.* **2003**, *42*, 2161−2089.
(7) Medalia, A. I. *Rubber Chem. Technol.* **1986**, *59*, 432−454.
(8) Guth, E. *J. Appl. Phys.* **1945**, *16*, 20−25.
(9) Siegfried, W.; Degussa, A. *Rubber Chem. Technol.* **1996**, *69*, 325−346.
(10) Karasek, L.; Sumita, M. *J. Mater. Sci.* **1996**, *31*, 281−289.
(11) Egerton, R. F. *Electron Energy-Loss Spectroscopy in the Electron Microscope*; Plenum: New York, 1996.
(12) Frank, J. In *Principles of Electron Tomography*; Frank, J., Ed.; Plenum Press: New York, 1992.
(13) Midglay, P. A.; Weyland, M. *Ultramicroscopy* **2003**, *96*, 413−431.
(14) Jinnai, H.; Ikehara, T.; Nishi, T. *Adv. Polym. Sci.* **2004**, *170*, 115−167.
(15) Dohi, H.; Kimura, H.; Kotani, M.; Kaneko, T.; Kitaoka, T.; Nishi, T.; Jinnai, H. *Polym. J.* **2007**, *39*, 749−758.
(16) Kawase, N.; Kato, M.; Nishioka, H.; Jinnai, H. *Ultramicroscopy* **2007**, *107*, 8−15.
(17) Spontak, R. J.; Williams, M. C.; Agard, D. A. *Polymer* **1988**, *29*, 387−395.
(18) Spontak, R. J.; Fung, J. C.; Braunfeld, M. B.; Sedat, J. W.; Agard, D. A.; Kane, L.; Smith, S. D.; Satkowski, M. M.; Ashraf, A.; Hadjuk, D. A.; Gruner, S. M. *Macromolecules* **1996**, *29*, 4494−4507.
(19) Laurer, J. H.; Hajduk, D. A.; Fung, J. C.; Sedat, J. W.; Smith, S. D.; Gruner, S. M.; Agard, D. A.; Spontak, R. J. *Macromolecules* **1997**, *30*, 3938−3941.
(20) Jinnai, H.; Nishikawa, Y.; Spontak, R. J.; Smith, S. D.; Agard, D. A.; Hashimoto, T. *Phys. Rev. Lett.* **2000**, *84*, 518−521.
(21) Yamauchi, K.; Takahashi, K.; Hasegawa, H.; Iatrou, H.; Hadjichristidis, N.; Kaneko, T.; Nishikawa, Y.; Jinnai, H.; Matsui, T.; Nishioka, H.; Shimizu, M.; Furukawa, H. *Macromolecules* **2003**, *36*, 6962−6966.
(22) Jinnai, H.; Yasuda, K.; Nishi, T. *Macromol. Symp.* **2006**, *245−246*, 170−174.
(23) Kaneko, T.; Suda, K.; Satoh, K.; Kamigaito, M.; Kato, T.; Ono, T.; Nakamura, E.; Nishi, T.; Jinnai, H. *Macromol. Symp.* **2006**, *242*, 80−86.
(24) Jinnai, H.; Sawa, K.; Nishi, T. *Macromolecules* **2006**, *39*, 5815−5819.
(25) Sugimori, H.; Nishi, T.; Jinnai, H. *Macromolecules* **2005**, *38*, 10226−10233.
(26) Wilder, E. A.; Braunfeld, M. B.; Jinnai, H.; Hall, C. K.; Agard, D. A.; Spontak, R. J. *J. Phys. Chem. B* **2003**, *107*, 11633−11642.
(27) Koster, A. J.; Ziese, U.; Verkleij, A. J.; Janssen, A. H.; de Jong, K. P. *J. Phys. Chem. B* **2003**, *104*, 9368−9370.
(28) Jinnai, H. *Nippon Gomu Kyokaishi* **2003**, *76*, 384−389.
(29) Shinbori, Y.; Jinnai, H.; Nishikawa, Y.; Kaneko, T.; Niihara, K.; Nishi, T. *Polym. Prepr. Jpn.* **2004**, *53*, 4231−4232.
(30) Niihara, K.; Kaneko, T.; Suzuki, T.; Sato, Y.; Nishioka, H.; Nishikawa, Y.; Nishi, T.; Jinnai, H. *Macromolecules* **2005**, *38*, 3048−3050.
(31) Kaneko, T.; Nishioka, H.; Nishi, T.; Jinnai, H. *J. Electron Microsc.* **2005**, *54*, 437−444.
(32) Belmont, A. S.; Sedat, J. W.; Agard, D. A. *J. Cell Biol.* **1987**, *105*, 77−92.
(33) Luther, P. K.; Lawrence, M. C.; Crowther, R. A. *Ultramicroscopy* **1988**, *24*, 7−18.
(34) Radermacher, M. In *Weighted Back-Projection Methods*; Frank, J., Ed.; Plenum Press: New York, 1992.
(35) Heidenreich, R. D.; Hess, W. M.; Ban, L. L. *J. Appl. Crystallogr.* **1968**, *1*, 1−19.
(36) Nishikawa, Y.; Jinnai, H.; Koga, T.; Hashimoto, T.; Hyde, S. T. *Langmuir* **1998**, *14*, 1242−1249.
(37) Nishioka, H.; Niihara, K.; Kaneko, T.; Yamanaka, J.; Inoue, T.; Nishi, T.; Jinnai, H. *Compos. Interfaces* **2006**, *13*, 589−603.
(38) Hon, A. A.; Busfield, J. J. C.; Thomas, A. G. In *Constitutive Models for Rubber III*; Busfield, J. J. C., Muhr, A., Eds.; Balkema: London, 2003.
(39) Busfield, J. J. C.; Jha, V. A. A. H. A. G. T. In *Constitutive Models for Rubber IV*; Kari, L. P.-E., Austrell, A. A., Eds.; Balkema: Leiden, 2005.
(40) Akutagawa, K.; Yamaguchi, K.; Yamamoto, A.; Heguri, H.; Jinnai, H.; Shinbori, Y. Manuscript in preparation.
(41) Tchoudakov, R.; Breuer, O.; Narkis, M.; Siegmann, A. *Polym. Eng. Sci.* **1996**, *36*, 1336−1346.
(42) Hammersley, J. M.; Handscomb, D. C. *Monte Carlo Methods*; Methuen: London, 1964.

MA071102D